Available online at www.sciencedirect.com
ScienceDirect
Ceramics International 37 (2011) 2543–2548
CERAMICS INTERNATIONAL
www.elsevier.com/locate/ceramint

Synthesis and characterization of spinel–forsterite nanocomposites

F. Tavangarian [a,b,*], R. Emadi [a]

[a] Department of Materials Engineering, Isfahan University of Technology, Isfahan 84156-83111, Iran
[b] Center of Applied Science and Technology, Entekhab Industrial Group, Isfahan 81668-33851, Iran

Received 23 March 2011; received in revised form 31 March 2011; accepted 31 March 2011
Available online 7 April 2011

Abstract

This is the first report of successful synthesis of pure spinel–forsterite nanocomposites from talc, alumina, and magnesium carbonate powders. Appropriate ratios of initial materials were mixed and mechanically activated in a planetary ball mill. The obtained powders were annealed at high temperatures. Pure spinel–forsterite nanocomposites with crystallites size in the range of 30–87 nm were obtained after 40 h of mechanical activation and subsequent annealing at 1200 °C for 1 h. The results of cold crushing strength (CCS) showed that the maximum strength of the fired spinel–forsterite bodies (~67 MPa) can be obtained in those samples with 10 wt.% spinel. The bulk density (BD) and apparent porosity (AP) of these samples were 1.46% and 17%, respectively.

Keywords: A. Calcination; B. Nanocomposites; C. Mechanical properties; D. Spinels

1. Introduction

Forsterite is a crystalline magnesium silicate belonging to the group of olivine with the chemical formula Mg_2SiO_4. Forsterite is a material of interest to engineers and designers, especially as an active medium for tunable laser [1,2]. It shows good refractoriness due to high melting point (~1890 °C), low thermal expansion and conductivity, good chemical stability and excellent insulation properties even at high temperatures [3].

Various composites were developed to improve the physicomechanical properties, strength, dielectric constant, thermal expansion, thermal conductivity and mechanical performance of forsterite ceramics. The properties are improved through addition of magnesium aluminate spinel, alumina, mullite, and partially stabilized zirconia [4]. Magnesium aluminate spinel ($MgAl_2O_4$) is one of the best-known and widely used polycrystalline materials on account of its attractive properties such as high melting point, high mechanical strength at elevated temperatures, high chemical inertness, and good thermal shock resistance [5–7]. These special properties make $MgAl_2O_4$ a potential candidate as a refractory material [8,9]. Mustafa et al. [4] investigated the effects of spinel phase on the mechanical properties of forsterite ceramic. They observed that the formation of spinel phase strongly improved cold crushing strength of forsterite bodies. However, the final products had some undesirable enstatite ($MgSiO_3$) phase. The presence of enstatite in forsterite could be detrimental to the high temperature properties of material because enstatite dissociates into the forsterite and a SiO_2-rich liquid formed at 1557 °C [10].

The aim of the present study is to synthesize pure spinel–forsterite nanocomposites from talc, magnesium carbonate and alumina powders without the detrimental presence of the enstatite phase. The sintering behavior and mechanical properties of spinel–forsterite bodies will be investigated as well.

2. Experimental procedures

2.1. Preparation of spinel–forsterite nanocomposites

Talc ($Mg_3Si_4O_{10}(OH)_2$) (98% purity, Merck), magnesium carbonate ($MgCO_3$) (98% purity, Aldrich) and alumina (Al_2O_3) (99% purity, Merck) were used as initial powders. In order to develop spinel–forsterite nanocomposites, various weight ratios of magnesium carbonate, talc and alumina powders were mixed together. The powder mixtures were mechanically activated for 40 h in a planetary ball mill (Fritsch P7 type) under ambient conditions. The milling media consisted of a hardened steel vial

* Corresponding author. Tel.: +98 311 3915725; fax: +98 311 3912752.
E-mail address: f_tavangarian@yahoo.com (F. Tavangarian).

0272-8842/$36.00
doi:10.1016/j.ceramint.2011.03.056

Table 1
Composition of initial powder mixtures in different samples.

Designation	S0	S10	S20	S30	S40	S50
Talc (gr)	7.81	7.09	6.35	5.61	4.85	4.07
$MgCO_3$ (gr)	8.69	8.57	8.46	8.34	8.22	8.10
Al_2O_3 (gr)	0	0.84	1.69	2.55	3.43	4.33

Table 2
Phase composition of the different samples after annealing at 1200 °C for 1 h.

Designation	SA0	SA10	SA20	SA30	SA40	SA50
Forsterite (wt.%)	100	90	80	70	60	50
Spinel (wt.%)	0	10	20	30	40	50

with five balls, each 20 mm in diameter and weighing 32.5 g. In all milling runs, the ball-to powder weight ratio was 10:1 and the rotational speed of the main disc was set at 500 rpm. The heat treatment of ball milled powders was carried out at 1000 and 1200 °C for 1 h in air. The amount of initial materials and the composition of different samples after annealing at 1200 °C for 1 h are demonstrated in Tables 1 and 2, respectively.

2.2. Preparation of bulk samples

To evaluate the effects of spinel phase on cold crushing strength (CCS), bulk density (BD), and apparent porosity (AP), the prepared spinel–forsterite nanopowders were uniaxially pressed into pellets in a hardened steel mould at a pressure of 100 MPa using 5 wt.% glycerin binder. Pellets of 12 mm in diameter and 12 mm long were prepared. For each experiment, three samples were prepared. The samples were sintered in a programmable resistance furnace under ambient condition at 1200 °C for 2 h with a heating/cooling rate of 5 °C/min. Table 3 shows the designation of prepared bulk samples. In this table, for instance, SB0 is obtained from SA0 powder.

Table 3
Designation of prepared bulk samples after annealing at 1200 °C for 2 h with a heating/cooling rate of 5 °C/min.

Designation	SB0	SB10	SB20	SB30	SB40	SB50
Obtained from (–) powder	(SA0)	(SA10)	(SA20)	(SA30)	(SA40)	(SA50)

2.3. Characterization of samples

The phase transformation were investigated by X-ray diffractometry (XRD) using a Philips X'PERT MPD diffractometer with Cu Kα radiation (λ = 0.154056 nm). The XRD patterns were recorded in the 2θ range of 20–80° (step size of 0.04° and time per step of 1 s). Williamson–Hall method was used to estimate the crystallites size of forsterite and spinel powders [11]. The morphology of prepared samples was studied by scanning electron microscopy (SEM) in a Philips XL30 at an acceleration voltage of 20 kV. The CCS of sintered pellets was investigated according to the ASTM standard (C0020-00R05) by a Hydraulic Testing Machine type Amsler model D3010/2E. The AP and BD of sintered pellets were measured according to Archimedes principle [12].

3. Results and discussion

The traditional synthesis method of forsterite and spinel is the ceramic one during which the reaction in solid phase at high temperatures between oxides (or hydroxides or salts) takes place. This process has several disadvantages; the most important ones are the low surface area and the chemical

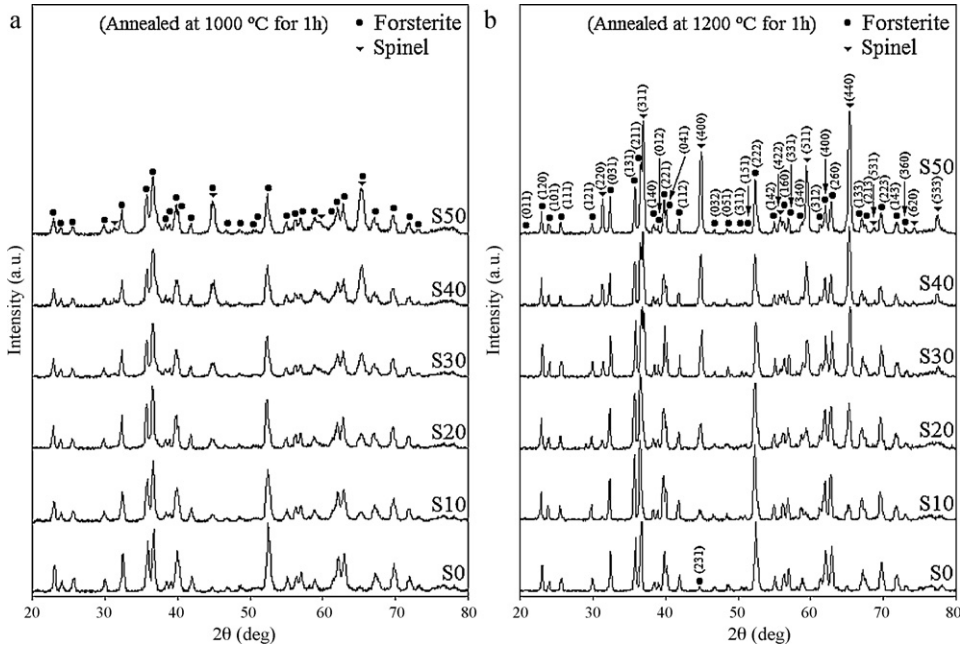

Fig. 1. X-ray diffraction patterns of various samples after 40 h mechanical activation and subsequent annealing at (a) 1000 and (b) 1200 °C for 1 h.

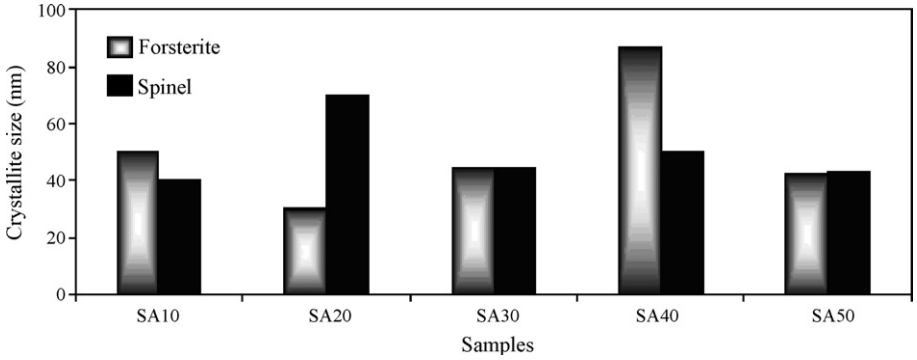

Fig. 2. Crystallite sizes of spinel and forsterite phases in different specimens.

inhomogeneity [13,14]. Mechanical activation is an efficient method to enhance the contact area and the interaction of the reactants, which increase the chemical homogeneity of the product and reduce the severity of thermal treatment [15,16].

As we showed in our previous studies [16–18], nanostructure forsterite and spinel powders can be obtained after 40 h of mechanical activation with subsequent annealing at 1200 °C for 1 h. The aim of the present work was to synthesize pure spinel–forsterite nanocomposites from the mixture of talc, magnesium carbonate, and alumina powders simultaneously. Hence, initial powders were milled for 40 h and then annealed at 1000 and 1200 °C for 1 h. Fig. 1a and b shows the XRD patterns of various samples (S0–S50) after 40 h of mechanical activation with subsequent annealing at 1000 and 1200 °C for 1 h, respectively. As can be seen in Fig. 1a, after mechanical activation of S0 for 40 h and subsequent annealing

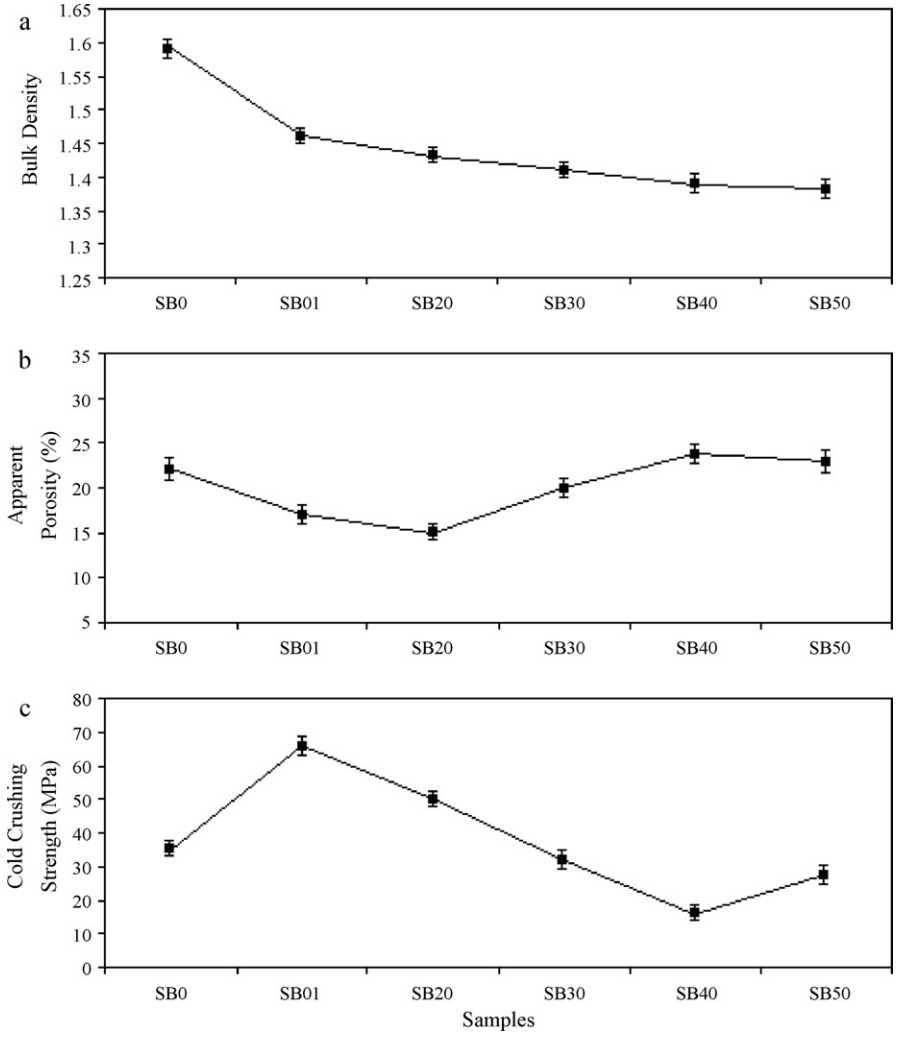

Fig. 3. (a) Bulk density, (b) apparent porosity, and (c) cold crushing strength of prepared bulk samples.

at 1000 °C for 1 h, just forsterite (XRD JCPDS data file No. 34-0189) phase could be obtained. By adding alumina to the initial powders of talc and magnesium carbonate (Table 1), spinel (XRD JCPDS data file No. 21-1152) could be formed besides forsterite phase. With increasing the weight percentage of alumina in the initial powders, the fraction of spinel phase increased from S10 to S50. It seems that spinel and forsterite phases were not fully crystallized due to the low annealing temperature. Many studies have reported that high temperatures (above 1000 °C) are needed for the complete crystallization of spinel phase [16,19–22]. Providing that spinel is not formed completely, the volume expansion (5–7%) accompanying the spinellization reaction can be detrimental to densification [21–23]. Therefore, to decrease the risk of volume expansion of spinellization reaction during the sintering process of bulk samples, the obtained powders after 40 h of mechanical activation were annealed at 1200 °C for 1 h (Fig. 1b). As can be seen in Fig. 1b, the XRD peaks intensity of spinel and forsterite phases increased in comparison with those samples that annealed at 1000 °C (Fig. 1a). This could be attributed to the better crystallization of spinel and forsterite phases. On the other hand, with increasing the annealing temperature, the width of XRD peaks decreased as a result of grain growth phenomenon occurring at higher annealing temperature [16]. No other phase was observed in the XRD patterns.

The crystallites size of spinel–forsterite nanopowders obtained by annealing of ball milled powders at 1200 °C for 1 h has been determined by Williamson–Hall equation [11]. The results are presented in Fig. 2. As can be seen, the crystallites size of spinel and forsterite phases was in the range of 30–87 nm. Except the crystallite size of forsterite phase in SA40 and spinel phase in SA20, the crystallite size of the other samples changed in a narrow-range.

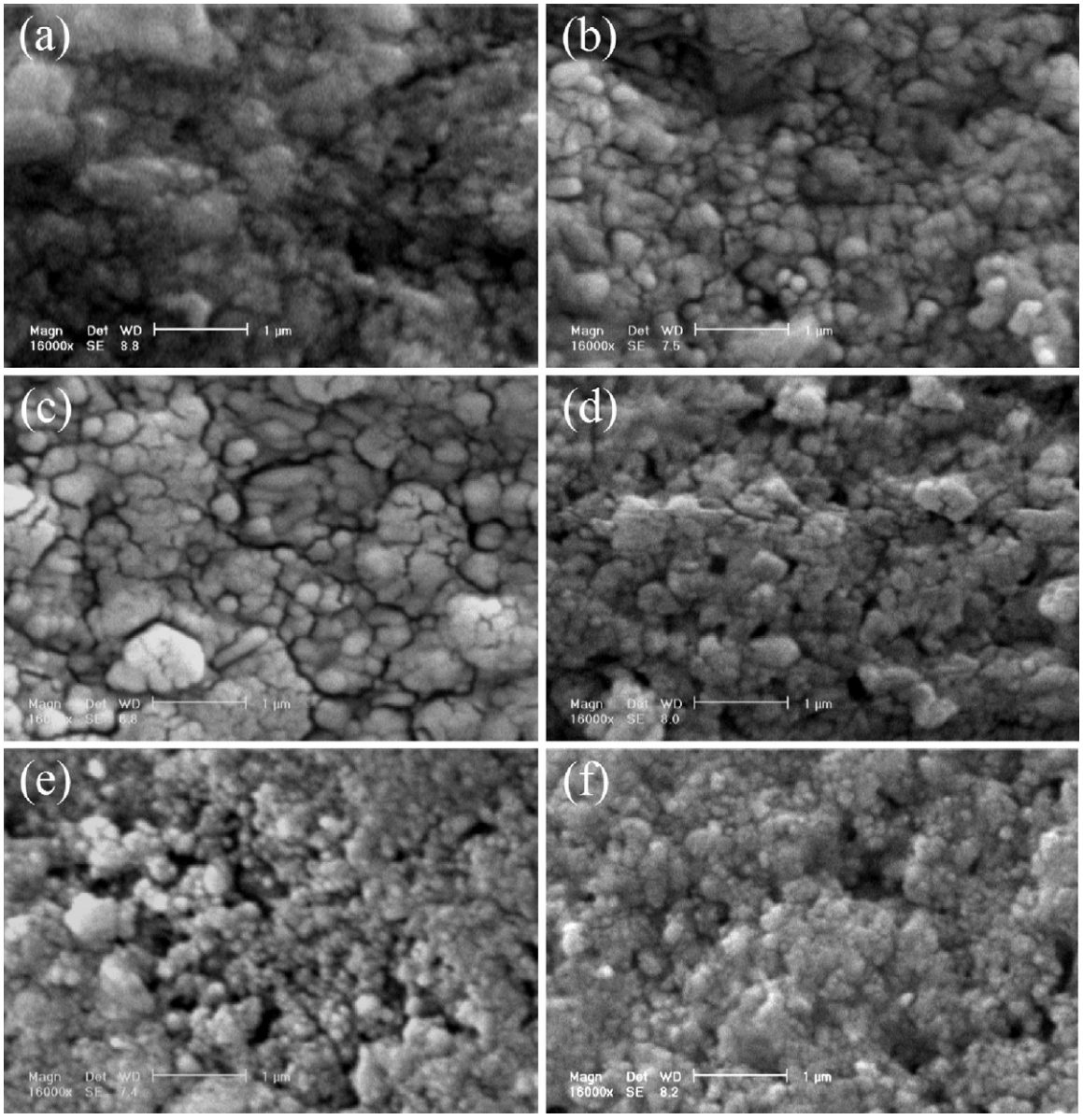

Fig. 4. SEM micrographs of (a) SB0, (b) SB10, (c) SB20, (d) SB30, (e) SB40, and (f) SB50.

Fig. 3a–c shows the results of BD, AP, and CCS of different samples. As can be seen, with increasing the weight percentage of alumina in the initial powders, BD decreased continuously as a result of the formation of spinel phase. In SB0, just forsterite phase was formed (with a melting point of 1890 °C) while in the other five samples (SB10–SB50), besides forsterite phase, spinel phase was developed (with a melting point of 2135 °C). Hence, BD decreased with increasing the weight percentage of spinel phase in the bulk samples.

AP decreased from SB0 to SB20 due to the formation of interlocked crystals of spinel and forsterite and the formation of a dense body with little pores [24,25]. On the other hand, AP increased from SB20 to SB40 due to the formation of higher amount of spinel phase. The formation of spinel phase is usually accompanied by some volume increase which may lead to weakening of the sample structure [26].

The results of CCS are shown in Fig. 3c. As can be seen, the presence of 10 percent of spinel in the forsterite structure increased the CCS of samples enormously. The CCS of SB0 was 35 MPa while SB10 had a CCS of about 67 MPa. With the formation of a slight amount of spinel in the forsterite structure, CCS increased about 2 times as a result of the formation of interlocked crystals of spinel and forsterite phases [24,25]. The formation of a higher amount of spinel in the bulk samples caused a decrease (from SB20 to SB40) and an increase (SB50) in the values of CCS. The reasons of the increase and decrease in the CCS values could be explained by the results obtained from AP (Fig. 3b). As can be seen, with decreasing the AP values, CCS increased and vice versa. The only exception in this case is BS20. In this sample, regardless of a decrease in the AP value, CCS also decreased. This could be clarified by the results obtained from SEM micrographs.

Fig. 4a–f shows the SEM micrographs of SB0–SB50, respectively. SB10 (Fig. 4b) exhibited relatively denser and more homogeneous grain-sized microstructure as compared with SB0 (Fig. 4a). This homogeneous microstructure as well as the lower AP (Fig. 3b) leads to the enhancement of the compressive strength [27]. On the other hand, we expected that BS20 showed a higher amount of CCS than BS10 due to the decrease in AP value. But CCS of this sample was lower than that of BS10. This could be explained by the SEM micrograph obtained from the surface of this sample. As can be seen in Fig. 4c, many cracks developed along the grain boundaries in the structure of BS20. This could be ascribed to the partial spinellization of prepared powders. As a result, in the preparing of bulk samples, spinellization occurred causing a volume expansion and therefore generating cracks in those samples [21–23]. The amount of spinel in BS10 is low and this phenomenon may have lower influence on the structure of the prepared bulk samples. But with increasing the amount of spinel phase in the final product, spinellization can play an important role in the amount of CCS. As can be seen in Fig. 4d and e, the morphology of surface changed gradually and a porous structure appeared. The higher amounts of AP in these specimens caused the lower values of CCS. In SB50 (Fig. 4f), a decrease in the particle size and AP may cause an increase in the value of CCS. These results are in a good agreement with those reported by Mustafa et al. [4].

4. Conclusions

1. Pure spinel–forsterite nanocomposites were prepared using talc, alumina, and magnesium carbonate powders.
2. Carefully adjusting the ratio of initial powders besides mechanical activation prevented the formation of enstatite phase which is detrimental to the high temperature properties of material.
3. The crystallites size of prepared spinel–forsterite nanocomposites was in the range of about 30–87 nm.
4. Cold crushing strength of those samples containing 10 and 20 wt.% spinel was higher than those samples without any spinel phase.
5. With the formation of 10 wt.% spinel in the forsterite structure, CCS reached the maximum value of 67 MPa, about 2 times higher than forsterite bulk specimens.
6. CCS decreased in those samples containing 20–40 wt.% spinel as a result of the formation of cracks, an increase in the apparent porosity, a decrease in the bulk density, and partial spinellization reaction.

References

[1] I.T. Mckinnie, R.Y. Choie, Efficient laser operation of heavily doped Cr4+:forsterite, Opt. Quant. Electron. 29 (1997) 605–610.
[2] L. Lin, M. Yin, C. Shi, W. Zhang, Luminescence properties of a new red long-lasting phosphor: Mg_2SiO_4:Dy^{3+}, Mn^{2+}, J. Alloys Compd. 455 (2008) 327–330.
[3] A. Saberi, Z. Negahdari, B. Alinejad, F. Golestani-Fard, Synthesis, characterization of nanocrystalline forsterite through citrate-nitrate route, Ceram. Int. 35 (2009) 1705–1708.
[4] E. Mustafa, N. Khalil, A. Gamal, Sintering and microstructure of spinel–forsterite bodies, Ceram. Int. 28 (2002) 663–667.
[5] C. Baudin, R. Martinaz, P. Pena, High temperature mechanical behaviour of stoichiometric magnesium spinel, J. Am. Ceram. Soc. 78 (1995) 1857–1862.
[6] I. Ganesh, S. Bhattacharjee, B.P. Saha, R. Johnson, K. Rajeshwari, R. Sengupta, M.V. Ramana Rao, Y.R. Mahajan, An efficient $MgAl_2O_4$ spinel additive for improved slag erosion and penetration resistance of high-Al_2O_3 and MgO-C refractories, Ceram. Int. 28 (2002) 245–253.
[7] I. Ganesh, S. Bhattacharjee, B.P. Saha, R. Johnson, Y.R. Mahajan, A new sintering aid for magnesium aluminate spinel, Ceram. Int. 27 (2001) 773–779.
[8] A. Troia, M. Pavese, F. Geobaldo, Sonochemical preparation of high surface area $MgAl_2O_4$ spinel, Ultrason. Sonochem. 16 (2009) 136–140.
[9] I. Ganesh, R. Johnson, G.V.N. Rao, Y.R. Mahajan, S.S. Madavendra, B.M. Reddy, Microwave-assisted combustion synthesis of nanocrystalline $MgAl_2O_4$ spinel powder, Ceram. Int. 31 (2005) 67–74.
[10] A. Douy, Aqueous synthesis of forsterite (Mg_2SiO_4) and enstatite ($MgSiO_3$), J. Sol–Gel Sci. Technol. 24 (2002) 221–228.
[11] G.K. Williamson, W.H. Hall, X-ray line broadening from filed aluminium and wolfram, Acta Metall. 1 (1953) 22–31.
[12] O. Engin, A.C. Tas, Manufacture of macroporous calcium hydroxyapatite bioceramics, J. Eur. Ceram. Soc. 19 (1999) 2569–2572.
[13] S.A. Bocanegra, A.D. Ballarini, O.A. Scelza, S.R. de Miguel, The influence of the synthesis routes of $MgAl_2O_4$ on its properties and behavior as support of dehydrogenation catalysts, Mater. Chem. Phys. 111 (2008) 534–541.

[14] G.W. Brindley, R. Hayami, Kinetics mechanism of formation of forterite (Mg_2SiO_4) by solid state reaction of MgO and SiO_2, Philos. Mag. 12 (1965) 505–514.
[15] F. Tavangarian, R. Emadi, Effects of fluorine ion and mechanical activation on nanostructure forsterite formation mechanism, Powder Technol. 203 (2010) 180–186.
[16] F. Tavangarian, R. Emadi, Synthesis and characterization of pure nanocrystalline magnesium aluminate spinel powder, J. Alloys Compd. 489 (2010) 600–604.
[17] F. Tavangarian, R. Emadi, Mechanical activation assisted synthesis of pure nanocrystalline forsterite powder, J. Alloys Compd. 485 (2009) 648–652.
[18] F. Tavangarian, R. Emadi, A. Shafyei, Influence of mechanical activation and thermal treatment time on nanoparticle forsterite formation mechanism, Powder Technol. 198 (2010) 412–416.
[19] E.N. Alvar, M. Rezaei, Mesoporous nanocrystalline $MgAl_2O_4$ spinel and its applications as support for Ni catalyst in dry reforming, Scripta Mater. 61 (2009) 212–215.
[20] E.A. Vasil'eva, L.V. Morozova, A.E. Lapshin, V.G. Konakov, A porous ceramic based on aluminomagnesium spinel, Russ. J. Appl. Chem. 75 (2002) 878–882.
[21] M.F. Zawrah, H. Hamaad, S. Meky, Synthesis and characterization of nano $MgAl_2O_4$ spinel by the co precipitated method, Ceram. Int. 33 (2007) 969–978.
[22] D. Mohapatra, D. Sarkar, Preparation of MgO–$MgAl_2O_4$ composite for refractory application, J. Mater. Process. Technol. 189 (2007) 279–283.
[23] H. Erkalfa, Z. Misirli, M. Demirci, Ç. Toy, T. Baykara, The densification and microstructural development of Al_2O_3 with manganese oxide addition, J. Eur. Ceram. Soc. 15 (1995) 165–171.
[24] K. Alessio, L. Hagemann, Behaviour of refractory products under constant and varying cyclic stress, Stahl-Eisen 11 (1990) 95–102.
[25] G. Routschka, C. Woehrmeyer, F. Gebhardt, Studies on the behaviour of magnesia, spinel and forsterite refractory bricks under simulated service conditions in the middle regions of oil-fired glass furnace regenerators, Part I. Corrosion tests and hot-mechanical behaviour of the test brick, Glastech-Ber. 63 (1990) 87–92.
[26] N.M. Khalil, Refractory aspects of Egyptian alum-waste material, Ceram. Int. 27 (2001) 695–700.
[27] M.F. Zawrah, A.B. Shehata, E.A. Kishar, R.N. Yamani, Synthesis, hydration and sintering of calcium aluminate nanopowder for advanced applications, C R Chim. (2011), doi:10.1016/j.crci.2010.11.004.